Protoplasma
DOI 10.1007/s00709-010-0137-5

ORIGINAL ARTICLE

On the nature and origin of the oxalate package in *Solanum sisymbriifolium* anthers

Hernán Pablo Burrieza · María Paula López-Fernández · Verónica Láinez · Teresita Montenegro · Sara Maldonado

Received: 11 December 2009 / Accepted: 15 March 2010

Summary This is a detailed study carried out in *Solanum sisymbriifolium* Lam. on the development of the circular cell cluster (CCC) during crystal deposition, as well as the composition of the crystals. Light microscopy and scanning and transmission electron microscopy (TEM) were used to characterize tissue throughout anther development. Energy dispersive X-ray analysis (EDAX) allowed the determination of the elemental composition of crystals that form in the CCC region, and infrared and x-ray diffraction analysis were used to specify the crystal salt composition. TEM analysis revealed that the crystals originated simultaneously within the vacuoles in association with a paracrystalline protein. Prior to the appearance of protein within vacuoles, protein paracrystals were visible in both rough endoplasmic reticulum and vesicles with ribosomes on their membranes. In vacuoles, paracrystals constitute nucleation sites for druse crystals formation. EDAX revealed that C, O, and Ca were the main elements, and K, Cl, Mg, P, S, and Si, the minor elements. X-ray powder diffraction of crystals detected the predominant presence of calcium oxalate, but also vestiges of calcite, quartz, and sylvite. The calcium oxalate coexisted in the three chemical forms, that is, whewellite, weddellite, and caoxite. Infrared spectrophotometry identified bands that characterize O-C-O, H-O, C-H bonds, all of calcium oxalate, and Si-O-Si, of quartz. These results were compared with studies of anthers carried out in other Solanaceae genera.

Keywords Ca oxalate · Ca crystals · Caoxite · Circular cell cluster · Druse crystals · EDAX · IR spectrophotometry · Oxalate package · Poricidal dehiscence · Protein paracrystals · *Solanum sisymbriifolium* · Solanaceae · Weddellite · Whewellite · X-rays powder diffraction

Introduction

The circular cell cluster (CCC), also known as the oxalate package, consists of highly specialized subepidermal cells subjacent to the stomium, each filled with numerous small calcium oxalate crystals. The cluster participates in the cell death process that unites the two pollen sacs of a theca into one large pollen chamber (Horner and Wagner 1980, 1992; Koltunow et al. 1990; Trull et al. 1991; Goldberg et al. 1993, 1995; D'Arcy et al. 1996; Beals and Goldberg 1997; Iwano et al. 2004; Sanders et al. 2005). This tissue is short-lived, and after cell death, cell walls degrade to leave a mass of druse crystals or raphide clusters. Crystal formation forms part of the anther developmental program. During dehiscence, crystals mixed with pollen arrive at the stigma. So far, in all taxa in which CCC has been reported, the informative distinction has been the type (raphides or druses) and nature (weddellite or whewellite) of crystals (D'Arcy et al. 1996).

Hernán Pablo Burrieza and María Paula López-Fernández contributed equally to the article.

H. P. Burrieza · M. P. López-Fernández · V. Láinez · S. Maldonado (✉)
Departamento de Biodiversidad y Biología Experimental,
Facultad de Ciencias Exactas y Naturales,
Universidad de Buenos Aires,
Pabellón 2, Ciudad Universitaria,
C1428EGA Ciudad de Buenos Aires, Argentina
e-mail: saram@bg.fcen.uba.ar

T. Montenegro
Departamento de Geología,
Facultad de Ciencias Exactas y Naturales,
Universidad de Buenos Aires,
C1428EGA Buenos Aires, Argentina

Published online: 07 April 2010

The Solanaceae is one of the 12 Angiosperm families that are conservative in the range of the CCC occurrence, and the oxalate package is found in at least one species of each of the six tribes in which the family has traditionally been divided (D'Arcy et al. 1996). There are four exceptions in which it is believed to be absent: the genera *Cestrum*, *Schwenckia*, *Nicandra*, and *Nierembergia* (D'Arcy et al. 1996). The tissue has been reported as present in genera with longitudinal dehiscence, as well as in some species of the genus *Solanum*, in which dehiscence is apical and poricidal (D'Arcy et al. 1996). In the *rbc*L phylogeny of Solanaceae proposed by Olmstead and Palmer (1992), the CCC is present in most of the genera that they studied, including *Schizanthus*, which is basal in their phylogenetic tree.

A particular feature of the CCC in Solanaceae is that each cell develops several druses within the central vacuole. This has not been observed in any other plant cell. However, neither the events associated with the intracellular formation of druse crystals nor the mechanisms that coordinate the cell differentiation and degeneration are known. Two transmission electron microscopy (TEM) studies have been carried out in *Capsicum annum* and *Nicotiana tabacum* by Horner and Wagner (1980) and Sanders et al. (2005), respectively, but the origin of these multiple druses remains obscure.

Chemical tests of druse crystals in Solanaceae have determined their composition as calcium oxalate (Namikawa 1919; Bonner and Dickinson 1989; Trull et al. 1991; Horner and Wagner 1980), present in its dihydrate form (weddellite) (Küster, 1956; Horner and Wagner 1992; Landolt and Kandeler 1987). However, Frey-Wyssling (1981) reported that the dense accumulation of very small crystals, which correspond to the oxalate package of Solanaceae, is in the monohydrate form of calcium oxalate (whewellite). To date, no other studies have been published that allow specification of the chemical composition of these crystals.

The species *Solanum sisymbriifolium* Lam. is native of America but is also present in Europe. It is commonly known as Sticky Nightshade or Fire-and-Ice plant. The species has light red to brown sharp spines covering the stems and leaves and is used as tincture or medicine by indigenous native peoples. This plant has also been used as a trap crop to protect potatoes from potato cyst nematode (USDA, ARS, National Genetic Resources 2008). It is an aggressive weed, with low sensitivity to the effect of systemic herbicide glyphosate. In this article, we have used different but complementary methods to study *S. sisymbriifolium* CCC tissue. In addition to a structural investigation using histochemical methods, scanning electron microscopy and TEM, an EDX analysis study of the elemental composition of crystals from CCC was also carried out. Infrared and x-ray analysis of crystals collected from these tissues were used as precise analytical methods to detect the crystal salt composition. Results were compared with studies on other Solanaceae anthers published to date.

Material and methods

Material

Anthers were studied from *S. sisymbriifolium* plant specimens growing on the campus of the Universidad de Buenos Aires, Buenos Aires City, Argentina. Material was collected in the floral stages: phase 1, stages -7 to -1; phase 2, stages +1 to +12, as described by Koltunow et al. (1990) and Beals and Goldberg (1997).

Methods

For light and TEM, excised anthers were first fixed for 2 hours at 4°C using a mixture of 2% paraformaldehyde and 1% glutaraldehyde in 0.1 M phosphate buffer, pH 7.2, then washed with 0.1 M phosphate buffer (pH 7.2) for 30 minutes and postfixed in 1% OsO_4 in water for 2 hours. Samples were then dehydrated in a graded ethanol–acetone series and embedded in Spurr's resin (Hawes 1994). Semithin sections (1 μm thick) and ultrathin sections were obtained for light microscopy (LM) and TEM, respectively, using an ultramicrotome (Reichert-Jung, Vienna, Austria) with a glass knife.

Semithin sections were stained with toluidine blue O (Sigma T 3260 CI 52040) and examined using an Axioskop 2 Zeiss photomicroscope equipped with phase contrast accessories to improve visualization of leaf tissues in unstained sections. Ultrathin sections were counterstained with uranyl acetate followed by lead citrate (Prego et al. 1998) and examined under a Zeiss EM 109 turbo (Zeiss, Wiesbaden, Federal Republic of Germany) transmission electron microscope operating at an accelerating voltage of 90 kV.

For histochemical studies, fresh sections and sections embedded in paraplast (Harris et al. 1994) were stained with toluidine blue O (Sigma T 3260 CI 52040), fast green FCF (Sigma F7252 CI 42053), and anilino-8-naphthalene sulphonic acid (Sigma A 8142 CI 82-76-8) to detect proteins (O'Brien and McCully 1981). As described in Harris et al. (1994), the presence of starch was determined on fresh sections with iodine potassium iodide (Sigma L 6146); the callose was detected with aniline blue (Sigma Aldrich 415049), and the lignin, in the fibrous thickening of the endothecial cell walls, was proven with phloroglucinol (Sigma P1178) and safranin O (Sigma S8884).

For environmental scanning electron microscopy (ESEM), crystals from fresh anthers were analyzed with a FEI/Philips

XL-30 ESEM equipped with an EDX analyzer. Sections of the anthers were examined in the environmental mode of the microscope.

For EDX analysis, an accelerating voltage of 20 kV and an analysis time of 60 seconds were routinely used.

For IR spectroscopy and x-ray diffractometry, crystalline material was directly isolated from fresh samples. After washing them several times using an ultrasonic cleaner, crystals were mechanically collected in a porcelain mortar, dried at room temperature, and finally disaggregated with an ultrasonic cleaner. The IR spectra were obtained by means of a Nicolet 8700 spectrophotometer in the spectral range between 4,000 and 400 cm^{-1} using the KBr pellet technique (4 mg of the powdered sample dispersed in 100 mg of KBr).

X-ray powder diffractograms were measured using a Siemens D5000 diffractometer.

Results

Crystals

The general aspect of crystals in anther sections, obtained by ESEM, is shown in Fig. 1a–c. The crystals are druses of 1 to 4 μm in diameter. EDX analysis revealed that the crystals contained C, O, and Ca as its main elements and Cl, K, Mg, P, S, and Si as minor elements. Figure 1d shows one of the spectra acquired.

The spectra obtained from crystalline powder by IR spectroscopy were well defined, as shown in Fig. 1e. The O-C-O stretching vibration of the whewellite presented double bands at 1,404.8 and 1616.1 cm^{-1}. The bands that characterize the H-O (at 3,275.5 cm^{-1}) and aliphatic C-H (between 2,919.1 and 2,850.3 cm^{-1}) bonds of weddellite were also detected (Echigo et al. 2005). The band at 1,319.9 cm^{-1} is due to whewellite. The finger print region shows peaks at 950 cm^{-1} (whewellite), 845 cm^{-1} (caoxite), and 650 cm^{-1} (caoxite) (Xie et al. 2007). One of the typical IR bands of quartz associated with Si-O-Si could be identified at 1,025.8 cm^{-1}. Because of its ionic bonds, potassium chloride is inert to IR radiation.

X-ray diffraction of extracted crystals allowed the complete identification of the mineral mixture. Figure 1f shows one of the diffractograms obtained. The analyses confirmed the presence of crystals of whewellite ($CaC_2O_4 .H_2O$), caoxite ($CaC_2O_4 .3H_2O$), weddellite ($CaC_2O_4 .2H_2O$), calcite ($CaCO_3 .6H_2O$), sylvite (KCl), and quartz (SiO_2).

CCC development

The development of the CCC was studied using both LM and TEM (Figs. 2, 3, 4 and 5). Stages of *S. sisymbriifolium* anther development were taken from studies of tobacco anther development by Koltunow et al. (1990) and Beals and Goldberg (1997).

When the wall layers, including the endothecium and tapetum, are formed (stages -6 to -5), cells destined to become the CCC are relatively uniform and can be distinguished by their position in the anther primordium alone (Fig. 2a). They are cytoplasmically rich in mitochondria, Golgi apparatus, ribosomes, and rough endoplasmic reticulum and contain small vacuoles (Fig. 3a–b). Plasmodesmata were observed between the CCC cells and stomium cells, indicating that the two tissues are connected by cytoplasmic channels during the process of cell differentiation.

By stage -3, that is, when callose deposition begins, there are a maximum of around 10 to 14 CCC cells in a transverse section (Figs. 2c and 3c–d). At this time, the small vacuoles fuse together to form a single large central vacuole and the cytoplasm compresses against the cell wall (Fig. 3e). Chloroplasts initiate degeneration, but the cytoplasm remains rich in mitochondria, Golgi apparatus, ribosomes, and rough endoplasmic reticulum (Fig. 4a–e). Active endocytosis was observed, with numerous vesicles originating in the plasma membrane and multivesicular bodies containing materials heading to vacuoles for degradation (Fig. 4c–e).

The number of CCC cells does not increase after stage -1 (meiosis in progress), and the cells of the CCC remain smaller than those flanking the region (Fig. 2d).

Crystal deposition initiates early in vacuoles (Fig. 3c–d), with the accumulation of protein in the lumen of the rough endoplasmic reticulum (Fig. 4a–b). Then, these protein deposits pinch off from the rough endoplasmic reticulum to form protein vesicles. Vesicles can be seen in the cytoplasm, surrounded by a rough endoplasmic reticulum-derived membrane with bound ribosomes (Fig. 4f–i). The protein in the vesicles exhibits a paracrystalline structure (Fig. 4h). Protein vesicles discharge in the vacuoles where membranes disorganize (Fig. 4d, j, k). In vacuoles, protein paracrystals become the nucleation sites for calcium oxalate deposition (Fig. 4j–k). Occasionally, deposition of calcium oxalate within the vesicle occurs before its separation from rough endoplasmic reticulum (Fig. 4d) or just upon arrival to the vacuole.

During meiosis (stages -1 to +1), salt deposition at nucleation sites in the central vacuole is very active (Figs. 3e and 4j–k), producing numerous crystals within the vacuole. By stage +3, that is, when microspores begin to vacuolize, the middle lamella has begun to dissolve (Fig. 4g, i). The process continues with cell death and the disintegration of their walls. During this time (around stage +10), the wall remnants and the druse crystals remain in the space previously occupied by the CCC (Figs. 4l and 5b–e). Druse crystals, optically anisotropic, were visualized with phase

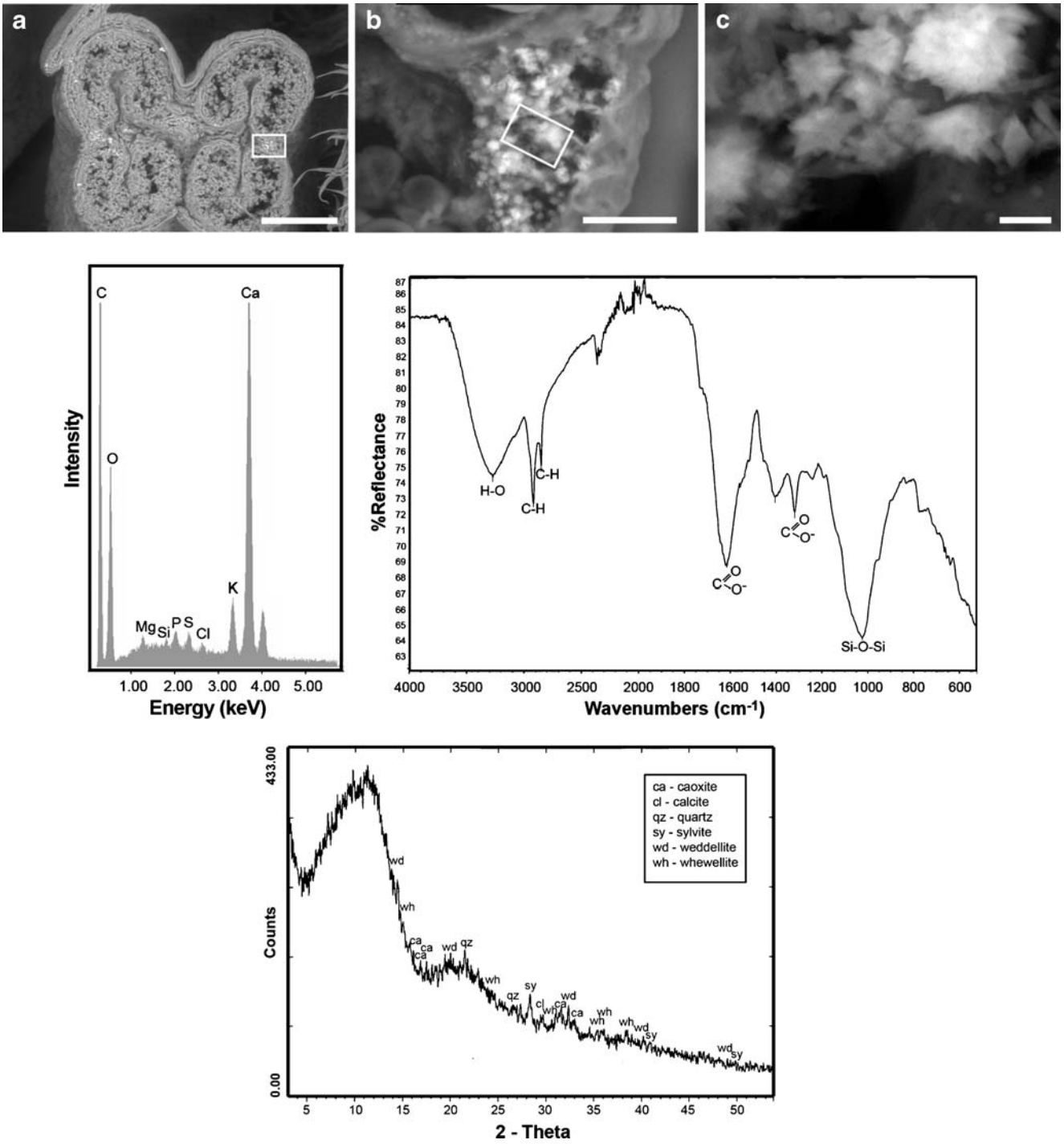

Fig. 1 **a–c** Druse crystals in a transverse section of *S. sisymbriifolium* anther as seen by ESEM at three levels of magnification (bars: 200, 10, and 2 μm, respectively). Panel **b** corresponds to the area delineated in panel **a**. Panel **c** corresponds to the area delineated in panel **b**. **d** One of the EDX analysis spectra of druses from *S. sisymbriifolium* anther. **e** IR spectrum of crystalline powder from *S. sisymbriifolium* anther CCC in the range of 4,000 to 500 cm^{-1}. X-ray diffraction pattern of the isolate from *S. sisymbriifolium*. *ca* caoxite (CaC_2O_4-$3H_2O$), *cc* calcite ($CaCO_3$- $6H_2O$), *qz* quartz (SiO_2), *sy* sylvite (KCl), *wd* weddellite (CaC_2O_4-$2H_2O$), *wh* whewellite (CaC_2O_4-H_2O)

contrast (Fig. 5b–e) and polarized light (data not shown). At the TEM level, the druses observed resembled "white stars." Actually, the white stars are the holes product of the sectioning, as the crystals are not sectioned (Fig. 4l). At this time, the group of crystals along the anther truly constitutes an oxalate package.

Together, these results indicate that the CCC differentiation program occurs between stages -3 and +4 and

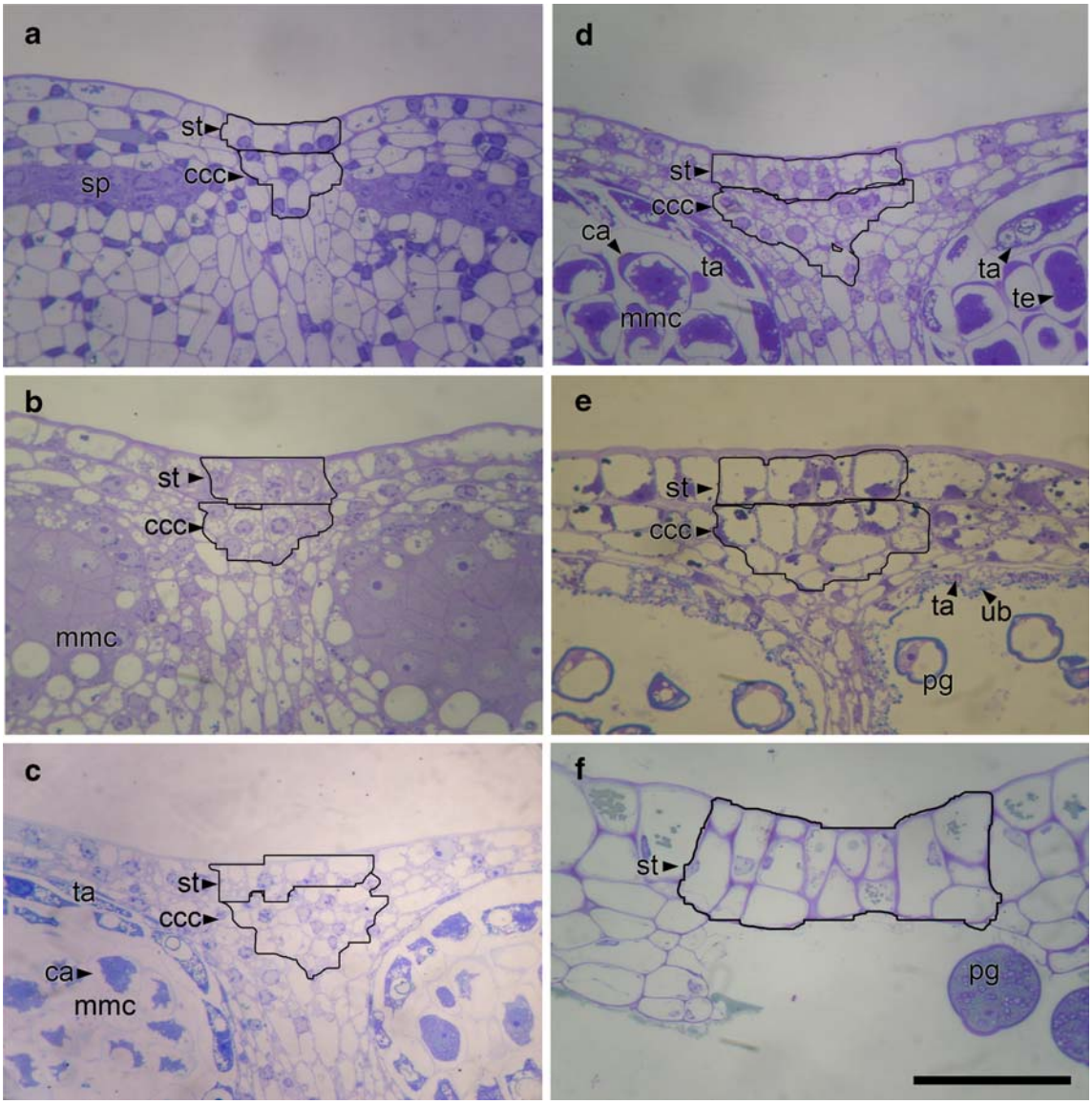

Fig. 2 LM images of transverse sections of *S. sisymbriifolium* anthers at different stages of development. Anther sections were fixed and embedded in Spurr's resin, as described in "Material and Methods." **a** Stage -5: Wall layers are formed, and the sporogenous tissue (*sp*) is differentiated; the CCC can be recognized by its position. **b** Stage -4; Microspore mother cells are formed from the sporogenous tissues. **c** Stage -3: Tapetum (*ta*) is differentiated and callose (*ca*) is deposited around the microspore mother cell (*mmc*). **d** Stage -1: Meiosis begins, and cells of the CCC differentiate. **e** Stage +4: Degeneration of the tapetum begins, and Ubisch bodies (*ub*) are identified on their tangential inner cell walls. Uninucleate and vacuolated pollen grains (i) can be seen. **f** Stage +10: In the stomium, some periclinal cell divisions occur; in the subjacent space previously occupied by the CCC, the debris of cell walls remains. At this stage, pollen grains are mature and full of reserves. The *black borders* delineate the stomium and the CCC cells. *ca* callose, *mmc* microspore mother cell, *pg* pollen grain, *st* stomium, *ta* tapetum, *te* tetrade. Bars: 50 μm

that deposition of calcium oxalate crystals and dissolution of the middle lamella mark the beginning of the CCC cell death program. Thus, the two programs partially overlap.

Differentiation and degeneration in stomium cells initiate more or less simultaneously with that of the CCC (Figs. 2 and 3). However, divisions in stomium cells continue until CCC cells degenerate. In fact, the pre-stomium formed by around four cells in a transverse section (Fig. 2a–b) undergo some anticlinal and periclinal divisions after stage +4, constituting a group of around 14 small cells at maturity (Figs. 2h and 5d–e). Stomium cells are markedly smaller in size in comparison with neighboring epidermal cells, remaining the narrowest site within the anther wall throughout anther development (Figs. 2f and 5c). Cell death occurs during later developmental stages. Cell walls do not degrade, but partial dissolution of the middle lamella is observed (Fig. 4l).

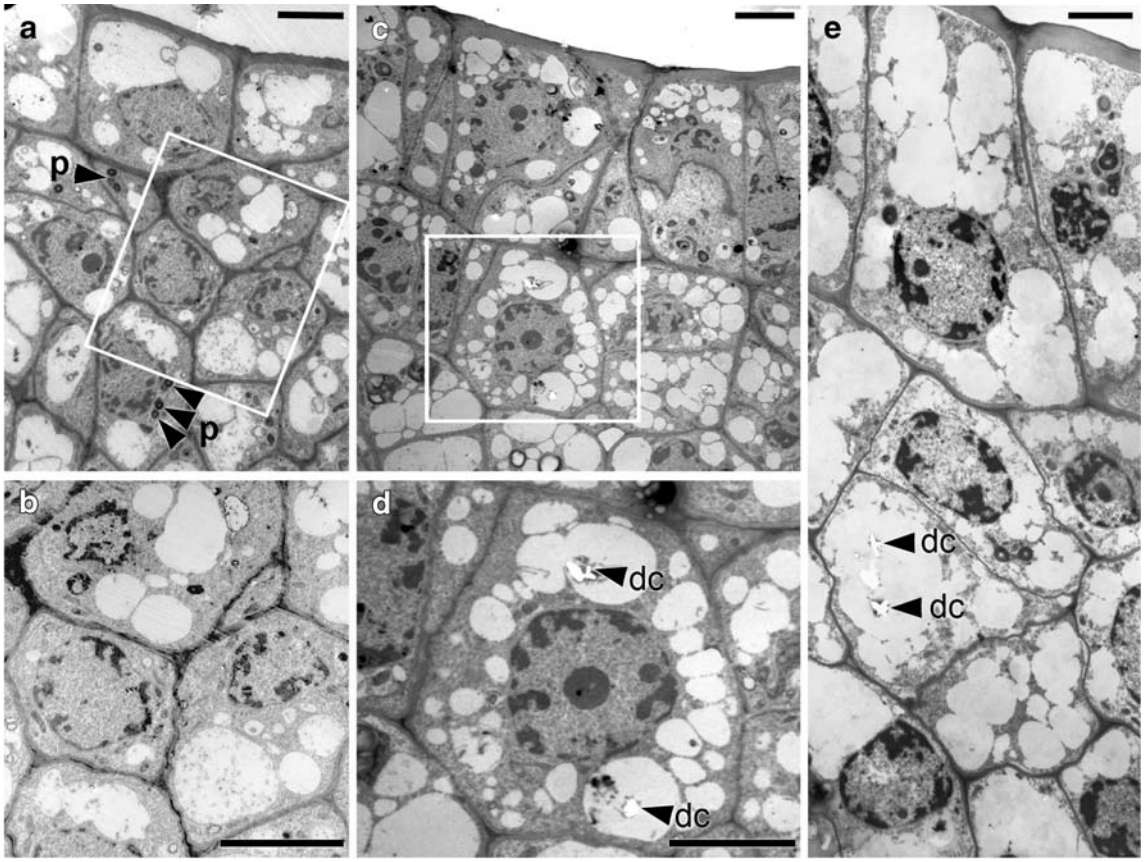

Fig. 3 **a–e** TEM images of transverse sections of *S. sisymbriifolium* anthers at different stages of development, showing stomium and CCC. **a** Stage -5. **b** Detail of panel **a**. **c** Stage -3. **d** Detail of panel **b**. **e** Stage -1. Anther sections from different stages of development were fixed and embedded in Spurr's resin, sliced into ultrathin sections, and stained with uranyl acetate followed by lead citrate, as described in "Material and Methods." *dc* druse crystals, *p* plastid. Bar: 10 μm

Figures 5 and 6a–b show sections of an anther shortly before dehiscence (stage +10). The series exhibits some differences according to the level of the sections (Fig. 5a). These are the following: (a) The endothecium is limited to the very short apical area of the anther, where pores are formed, and cells with thickened walls develop only at the apical end of all the tissues surrounding the pore (Figs. 5b–e and 6a–b); (b) at maturity, the cell death process in the CCC fuses the two pollen sacs of the theca into one large pollen chamber, except in a very short basal region where the CCC does not develop and the septum remains intact (Fig. 5f–g).

At dehiscence (stage +12), crystals mixed with pollen are liberated (Fig. 6c–d) and transported to the stigma by pollinators. In the stigma, crystals were observed unaltered in structure and elemental composition (Fig. 7a–b).

Discussion

In this study, we characterized the development and degeneration of the CCC during anther development in *S. sisymbriifolium*. In the genera of Solanaceae in which dehiscence is longitudinal, the CCC could play some role in the dehiscence process (Sanders et al. 2005), but in *S. sisymbriifolium*, as in most species of *Solanum* in which dehiscence is apical and poricidal (D´Arcy et al. 1996), it is possible to infer that CCC tissue is not associated with dehiscence. It is not clear if the CCC is present in all species of *Solanum* because in the 30 species studied by Carrizo et al. (2008), there is no mention of the presence of

Fig. 4 **a–e** TEM images of *S. sisymbriifolium* CCCs from anthers at different stages of development, showing both the process of endocytosis and the origin of paracrystalline protein. **f–i** Structure of protein vesicles. **j–k** Initial crystal deposition in vacuole. **l** Detail of the stomium, by stage +10, showing the oxalate package free in the site previously occupied by the CCC. Anther sections from different stages of development were fixed and embedded in Spurr's resin, sliced into ultrathin sections, and stained with uranylacetate followed by lead citrate, as described in "Material and Methods." *ch* chromatin, *dc* druse crystal, *ev* endocytic vesicle, *g* Golgi apparatus, *m* mitochondrion, *mb* multivesicular body, *ml* middle lamella, *pg* pollen grain, *r* ribosome, *rer* rough endoplasmic reticulum, *s* starch, *v* vacuole. *Asterisks* indicate protein paracrystals. Bars: 2 μm (**a-g, i**), 1 μm (**h**), 4 μm (**j-l**)

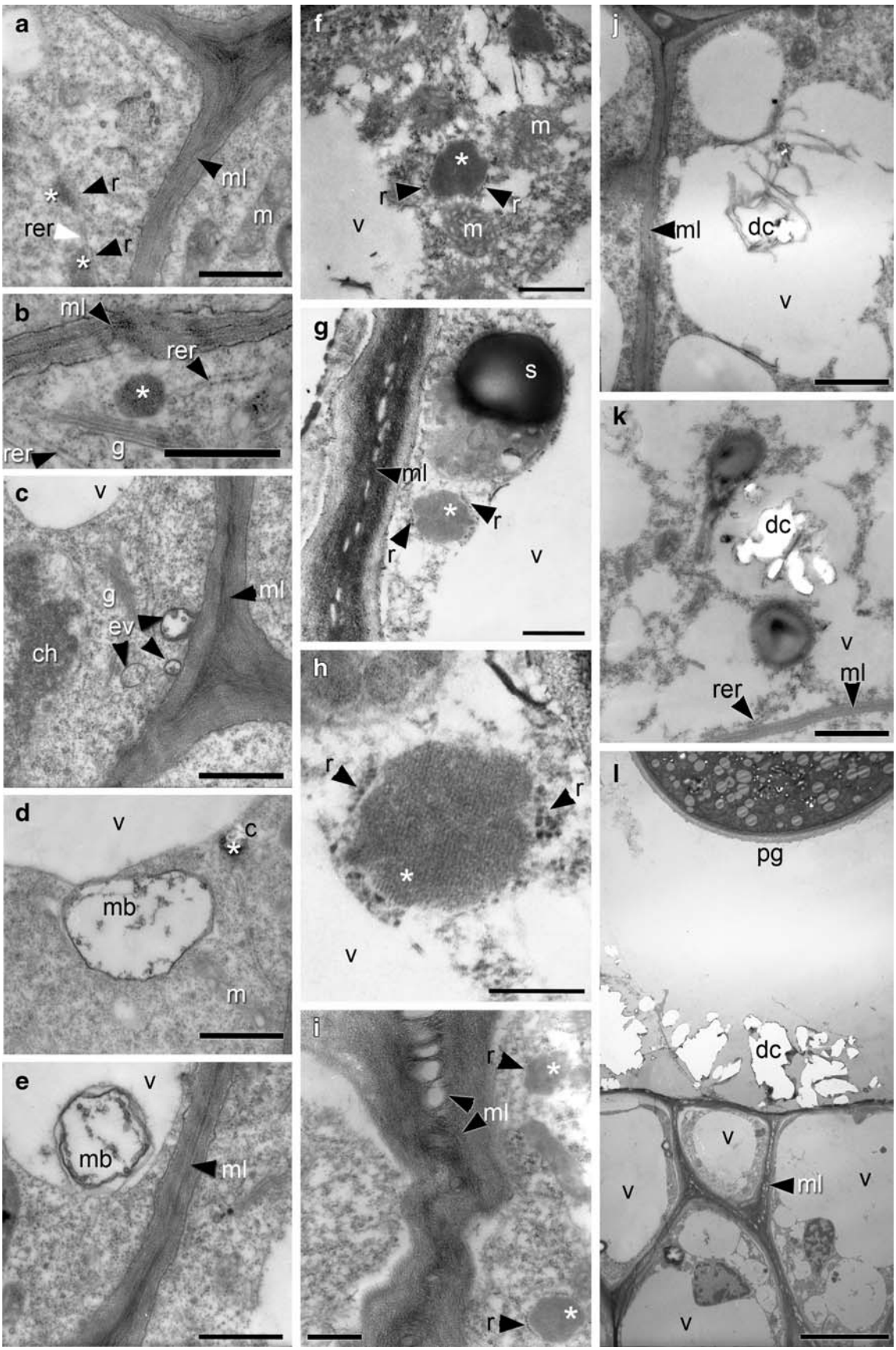
a
r
ml
*
rer
r
m
*
b
ml
rer
*
rer
g
c
v
g
ml
ev
ch
d
v
c
*
mb
m
e
v
mb
ml
f
m
*
r
r
v
m
g
s
ml
*
r
r
v
h
r
r
*
v
i
r
*
ml
r
*
j
ml
dc
v
k
dc
v
ml
rer
l
pg
dc
v
v
ml
v
v

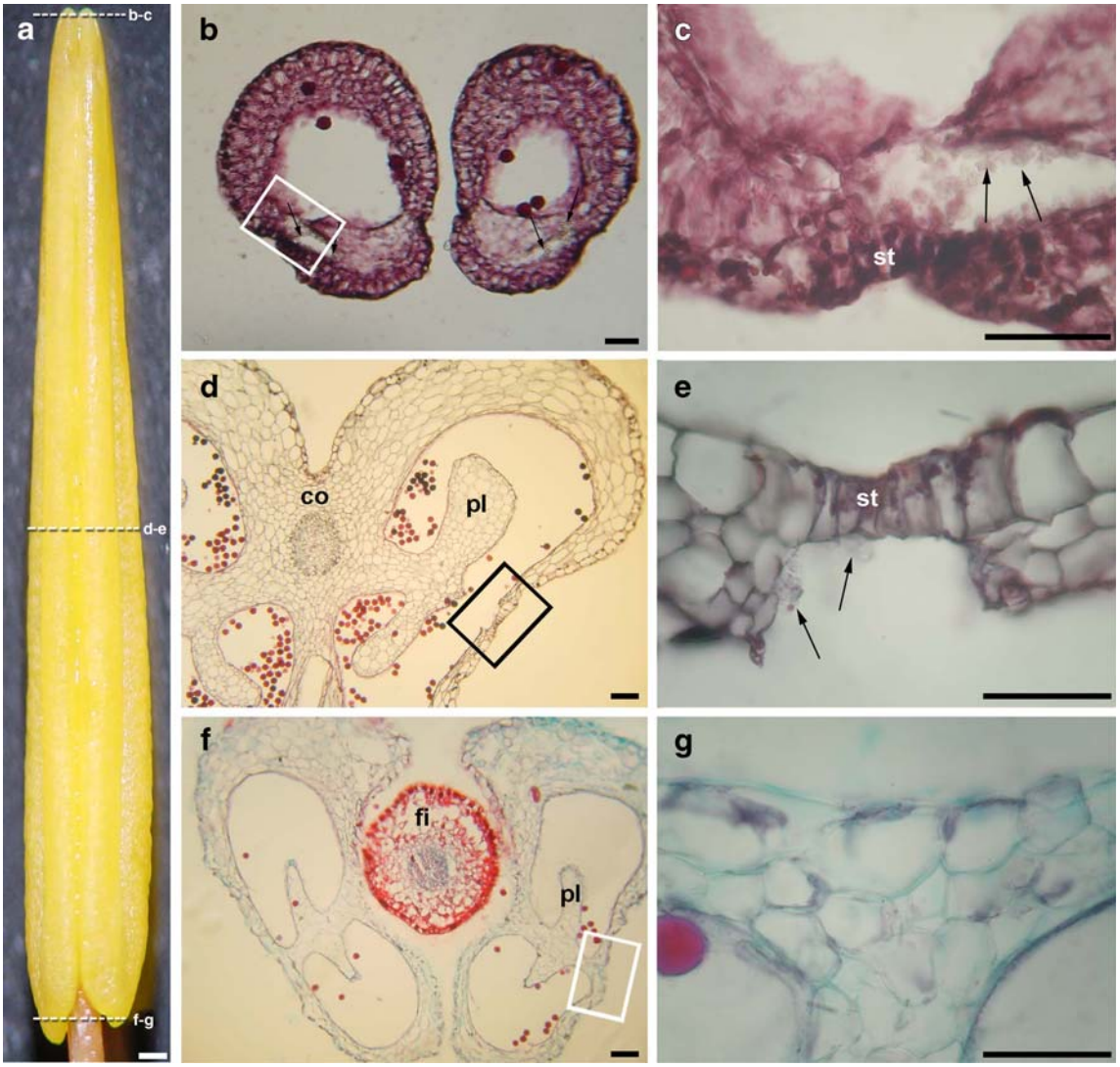

Fig. 5 **a** *S. sisymbriifolium* anther corresponding to stage +10, as seen with a stereoscopic microscope. **b-g** LM transverse sections of anthers. The images were obtained from anthers fixed and embedded in paraplast and stained with safranin and fastgreen, as described in "Material and Methods." **b** Apical region of the anther in the plane indicated in panel **a**. **c** Detail of panel **b** showing the dehiscent area. **d** Middle region of the anther in the plane indicated in panel **a**; in this image, the placentoid tissue (*pl*), a structure characteristic of Solanaceae anther, can be observed. **e** Detail of panel **d**. **f** Basal region of the anther in the plane indicated in panel **a**; in this plane, the filament (*fi*) is separated from the thecae, and the placentoids (*pl*) are visible. **g** Detail of panel **f**. *co* connective, *fi* filament, *pl* placentoid. *Arrows* indicate the druse crystals. Bars: 400 μm μm (**a**), 100 μm (**b, d, f**), 50 mm (**c, e, g**)

this cluster or the occurrence of crystallization in tissues subjacent to the stomium.

In this study, we found that the CCC is hypodermal in origin, being subhypodermal only in a short basal region of the anther. In most taxa of Solanaceae, the CCC is hypodermal except for *Cyphomandra*, many species of *Solanum* subgenus *Leptostemonum*, and some species of *Lycianthes*, in which it is subhypodermal (D'Arcy et al. 1996).

Crystal formation in the CCC is part of the anther developmental program. This event is unique and differs from crystal formation in other plant tissues, where, according to Xingxiang et al. (2003), the process is considered to be a high-capacity mechanism for regulating Ca. During this process, many small druse crystals fill the vacuoles of the CCC cells. These cells are also different from the other known druse idioblasts, in which just one druse crystal is formed per cell. The CCC has been studied at the ultrastructural level in *C. annum* (Horner and Wagner 1980, 1992), tobacco (Sanders et al. 2005), *Vassobia breviflora*, and *Witheringa solanacea* (D´Arcy et al. 1996). In the latter two species, studies have reported that during development, there is no proliferation of smooth or rough endoplasmic reticulum, unusual amounts of mitochondria, and any evidence of particular organelles, as well as that druses are formed in small vacuoles that then

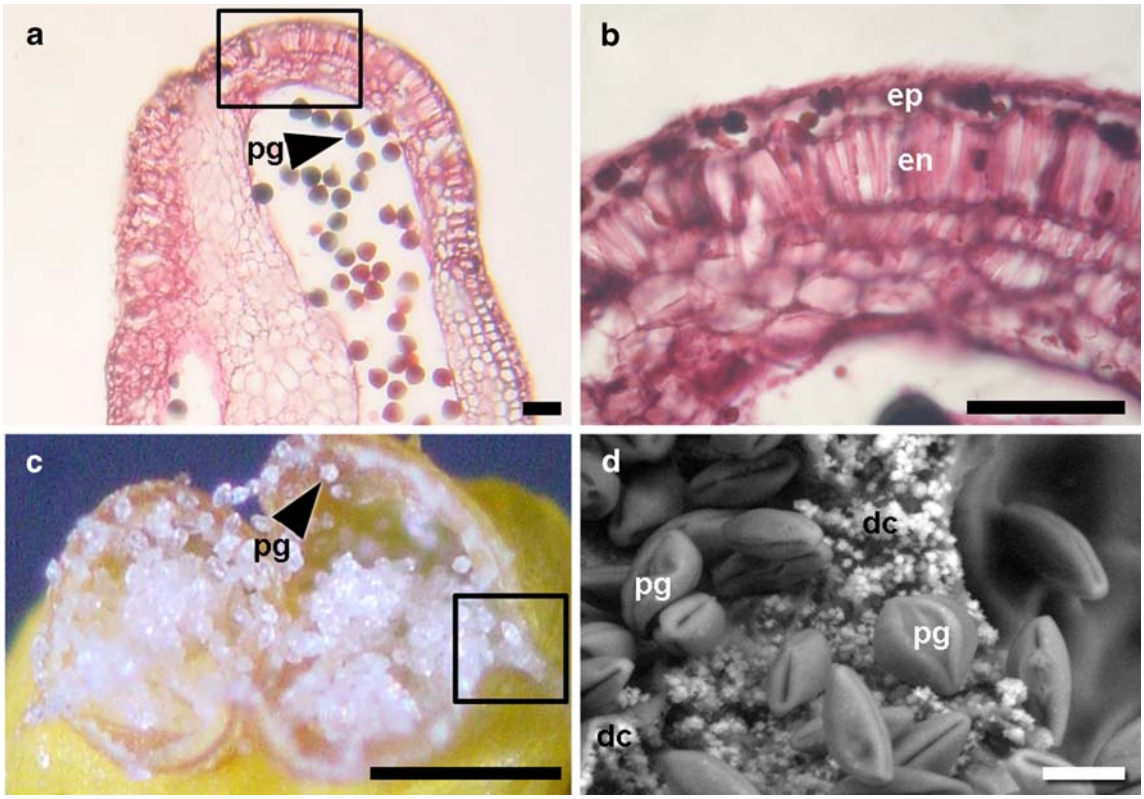

Fig. 6 **a–b** Apical region of an *S. sisymbriifolium* anther. Endothecium (*en*) develops only in the apical region of the anther; cell wall thickenings are observed in anther embedded in paraplast and stained with safranin, as described in "Material and Methods." **c–d** During dehiscence, druse crystals (*dc*) can be seen mixed with pollen grain (*pg*). The ESEM image was obtained from a fresh anther using the environmental mode of the microscope, as described in "Material and Methods." *dc* druse crystals, *en* endothecium, *ep* epidermis, *pg* pollen grain, *st* stomium. Panel **b** corresponds to the area delineated in panel **a**. *dc* druse crystal, *en* endothecium, *ep* epidermis, *pg* pollen grain. Bars: 50 μm (**a, b**), 250 μm (**c**), 10 μm (**d**)

combine to form the large vacuole. With regard to tobacco, Sanders et al. (2005) only mention that calcium oxalate druse crystals are present in large vacuoles at stage +2, when cytoplasm is compressed against the cell wall and the nucleus appears shrunken and distorted. In their study of *Capsicum annuum*, Horner and Wagner (1980) find that druses are associated with membrane complexes and paracrystalline bodies, the latter forming nucleation sites for crystal formation.

Our studies on *S. sisymbriifolium* anther development revealed that (1) crystal deposition begins in stage -3; (2) during this stage, the cells of the CCC present dense cytoplasms, with small vacuoles, very rich in rough endoplasmic reticulum and mitochondria; (3) proteins with a paracrystalline structure accumulate within the lumen of the rough endoplasmic reticulum cisternae and then pinch off from the rough endoplasmic reticulum to form protein vesicles that are surrounded by a rough endoplasmic reticulum-derived membrane; (4) protein vesicles are discharged in the vacuoles (small or large vacuoles, depending on the developmental stage); (5) in vacuoles, the paracrystalline structures constitute nucleation sites for calcium oxalate deposition. In regard to the latter, we also proved that in *S. sisymbriifolium*, as in *C. annum*, the multiple nucleation sites are located in the vacuole; (6) active endocytosis is associated with the deposition of protein paracrystals in the vacuole. To this effect, vesicles originating in plasma membranes and multivesicular bodies discharging in vacuoles both constitute evidence of the endocytic pathway, according to Staehelin and Newcomb (2000).

In water lettuce (*Pistia stratiotes*) leaves, Xingxiang et al. (2003) demonstrate that a specific Ca-binding protein exists as an integral component of Ca oxalate crystals. This protein is associated with the developing crystals and transported to the vacuole by the Golgi apparatus. In *S. sisymbriifolium* anthers, we found that the structures that deliver proteins to the vacuoles are vesicles originated from rough endoplasmic reticulum and that exhibit ribosomes on their membranes.

In *S. sisymbriifolium*, we found plasmodesmata connections between cells of the stomium and CCC during early stages of development. The presence of plasmodesmata indicates possible interactions between the two tissues

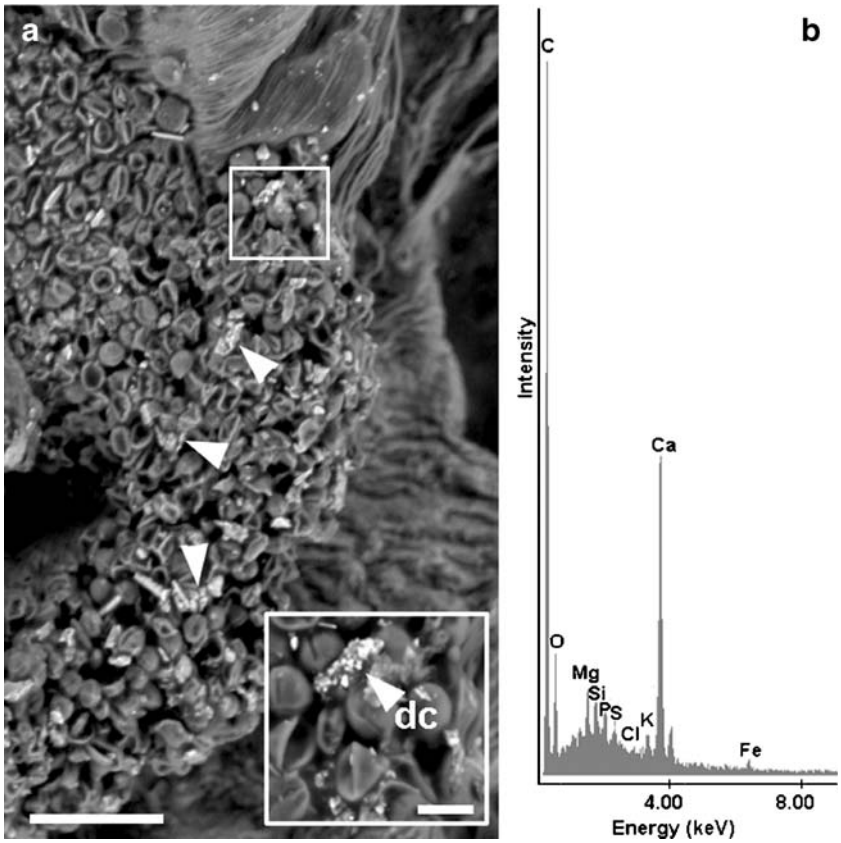

Fig. 7 **a** ESEM image of the stigma of an *S. sisymbriifolium* flower after pollination. Packages of crystal and single crystals are mixed with pollen grains. *Arrows* indicate druse crystal packages. The ESEM image was obtained from a fresh pistil using the environmental mode of the microscope, as described in "Material and Methods." **b** One of the EDX analysis spectra of crystals found for *S. sisymbriifolium* stigma is shown. *dc* druse crystal. Bars: 100 m (**a**), 20 μm (insert)

when CCC and stomium become specialized. During CCC degeneration, plasmodesmata disappeared. The occurrence of plasmodesmata has also been reported in tobacco in Sanders et al. (2005).

Stomium differentiation concludes once the CCC has disappeared, and stomium cell death occurs in the absence of a CCC. Thus, the CCC is not required for cellular processes that occur within the stomium during most of phase 2 of anther development. These observations are consistent with the hypothesis of Sanders et al. (2005) that the CCC and the stomium differentiate and function independently of each other after they are specified. According to Goldberg et al. (1993), the differentiation and degeneration of the CCC and stomium that occur within the notch region must be coordinated with other events that occur within the anther, for example, pollen grain formation, tapetal cell degeneration, expansion of wall and epidermal layers, deposition of fibrous bands in the connective and endothecium, and connective cell degeneration. In addition, anther development and dehiscence must be timed with events that occur within other floral organs (i.e., sepals, petals, and pistil) so that successful pollination and fertilization can take place when the flower opens.

In *S. sisymbriifolium*, we detected partial dissolution of the middle lamella. We also observed endothecial cells with wall thickenings restricted to the apical end of the anther. We inferred that both characters are derived characters, present here as relicts of the longitudinal dehiscence.

On the other hand, the lignin cell wall thickenings were observed only after stage +3 of phase 2 of anther development. In addition, in tobacco anther, endothecial cells generate wall thickenings, or fibrous bands, at the same stage of phase 2 of anther development (Sanders et al. 2005).

Although the crystals of the CCC are reported to be calcium oxalate, there have been few studies to determine its nature. In the Solanaceae family, chemical tests have been conducted on CCC crystals in *C. annum*, *Lycopersicum esculentum*, *Nicotiana alata*, *N. tabacum*, *Petunia violacea*, *Physalis allkekengii*, *Schizanthus pinnatus*, *Solanum nigrum*, *Solanum dulcamara*, *Solanum tuberosum*, and *Solanum melongena*, determining their composition as calcium oxalate (Namikawa 1919; Bonner and Dickinson 1989; Trull et al. 1991; Horner and Wagner 1980; and D'Arcy et al. 1996). As revealed by x-ray diffraction, druses are in the dihydrate form of calcium oxalate (Horner and Wagner 1992). However, Frey-Wyssling (1981) reported that these crystals correspond to the monohydrate form. Our studies on *S. sisymbriifolium* using IR spectrophotometry and x-ray diffraction proved that crystals are found in all forms (trihydrate, dihydrate, and monohydrate) of calcium oxalate (caoxite, weddellite, and whewellite, respectively), along with calcite, quartz, and sylvite.

In *L. esculentum*, Bonner and Dickinson (1989) identified by energy dispersive x-ray analysis (EDAX) Ca, P, S, and K during development. However, after cell death, P, S and K are present in only relatively small amounts, with Ca becoming almost exclusive. In *C. annum*, Horner and Wagner (1992) determined the absence of P. We carried out an EDAX analysis of crystals in *S. sisymbriifolium* at dehiscence in which Cl, K, Mg, P, S, and Si were always found as minor elements. Concerning calcium oxalate purity, D'Arcy et al. (1996) found that crystals in different taxa vary in appearance, which they attribute to differences in chemical composition, particularly the addition or substitution of Ca by small quantities of other elements. We infer that differences among crystal forms found in diverse Solanaceae species (D'Arcy et al. 1996) could be supported by both the proportion of each form of calcium oxalate to the others (mono-, di-, and trihydrate) and the presence of salts and cations as "impurities."

In plant species containing an oxalate package, druse crystals are taken up along with the pollen by pollinators and mixed with pollen grains (Iwano et al. 2004). The presence of calcium oxalate crystals in the stigma has recently been shown to enhance the pollination process by supplying calcium ions (Iwano et al. 2004). In anthers that open lenghwise, crystals mixed with pollen grains are brushed onto the pollinator that touches the anther. This is probably as consequence of sonication by insects during pollination (Harder and Barclay 1994; Harter et al. 2002).In *S. sisymbriifolium*, with apical and poricidal anthers, we revealed that crystals mixed with pollen are liberated and transported to the stigma by pollinators. However, we also observed that in the stigma they remained unaltered in structure and elemental composition.

Conclusions

Because the events that occur during anther development are highly consistent within the Solanaceae family, it would make sense that the origin of druse crystals be similar in all cases, that is, crystalline protein produced in the rough endoplasmic reticulum is transported to the vacuole via vesicles; in vacuoles, deposits of crystalline protein constitute the nucleation sites for calcium oxalate deposition. This was our major finding. It was also important to demonstrate that the three forms of calcium oxalate were present in the druses, perhaps initially as trihydrate, with transformation to di- and monohydrate by dehydration. In addition, the presence of other salts and cations was proven. However, it is left to future investigations to determine the molecular processes and genes that control the synthesis of these druse crystals and the characteristics and role of the crystalline protein in salt deposition.

Acknowledgements This work was supported by a grant from the Agencia Nacional de Promoción Científica y Tecnológica, (PICT - 2008-00144 for SM) and Universidad de Buenos Aires (UBACYT - X125) (SM). S.M., T.M., and V.L. are members of the Consejo Nacional de Investigaciones Científicas y Técnicas. H.B. and M.P.L.F. are supported by a Universidad de Buenos Aires doctoral research fellowship. We thank Pablo Picca for assistance with taxonomic assistance.

Conflict of interest The authors declare that they have no conflict of interest.

References

Beals TP, Goldberg RB (1997) A novel cell ablation strategy blocks tobacco anther dehiscence. Plant Cell 9:1527–1545

Bonner LJ, Dickinson HG (1989) Anther dehiscence in *Lycopersicum sculentum* Mill. New Phytol 113:97–115

Carrizo García C, Matesevach M, Barboza G (2008) Features related to anther opening in *Solanum* species (Solanaceae). Bot J Linn Soc 158:344–354

D'Arcy WG, Keating RC, Buchmann SL (1996) The calcium oxalate package or so-called resorption tissue in some angiosperm anthers. In: D'Arcy WG, Keating RC (eds) The anther: form, function and phylogeny. Cambridge University Press, Cambridge, pp 159–191

Echigo T, Kimata M, Kyono A, Shimizu M, Hatta T (2005) Re-investigation of the crystal structure of whewellite [Ca(C2O4). H2O] and the dehydration mechanism of caoxite [Ca (C2O4).3H2O]. Mineral Mag 69:77–88

Frey-Wyssling A (1981) Crystallography of the two hydrates of crystalline calcium oxalate in plants. Am J Bot 68:130–141

Goldberg RB, Beals TP, Sanders PM (1993) Anther development: basic principles and practical applications. Plant Cell 5:1217–1229

Goldberg RB, Sanders PM, Beals TP (1995) A novel cell-ablation strategy for studying plant development. Philos Trans R Soc B: Biol Sci 350:5–17

Harder LD, Barclay RMR (1994) The functional significance of poricidal anthers and buzz pollination: controlled pollen removal from *Dodecatheon*. Funct Ecol 8:509–517

Harris N, Spence J, Oparka KJ (1994) General and enzyme histochemistry. In: Harris N, Oparka KJ (eds) Plant cell biology - a practical approach. IRL Press at Oxford University Press, Oxford, pp 51–68

Harter B, Leistikow C, Wilms W, Truylio B, Engels W (2002) Bees collecting pollen from flowers with poricidal anthers in a south Brazilian Araucaria forest: a community study. J Apic Res 41:9–16

Hawes C (1994) Electron microscopy. In: Harris N, Oparka KJ (eds) Plant cell biology - a practical approach. IRL Press at Oxford University Press, Oxford, pp 69–96

Horner HT, Wagner BL (1980) The association of druse crystals with the developing stomium of *Capsicum annuum* (Solanaceae) anthers. Am J Bot 67:1347–1360

Horner HT, Wagner BL (1992) Association of four different calcium crystals in the anther connective tissue and hypodermal stomium of *Capsicum annuum* (Solanaceae) during microsporogenesis. Am J Bot 79:531–541

Iwano M, Tetsuyuki E, Shiba H, Takayama S, Isogai A (2004) Calcium crystals in the anther of petunia: the existence and biological significance in the pollination process. Plant Cell Physiol 45:40–47

Koltunow AM, Truettner J, Cox KH, Wallroth M, Goldberg RB (1990) Different temporal and spatial gene expression pattern occur during anther development. Plant Cell 2:1201–1224

Küster E (1956) Oxaltkristalle. In: Die Pflanzenzelle, 3rd edn. Gustav Fischer Verlag, Jena, pp 492–506

Landolt E, Kandeler R (1987) The family Lemnaceae—a monographic study. Veroeff Geobot. Inst. ETHS Rüberl, Zurich

Namikawa I (1919) Ueber das Oeffnen der Antheren bei einigen Solanaceen. Bot Mag Tokyo 33:385–396

O'Brien TP, Mc Cully NE (1981) The study of plant principles and selected methods Termarcarphi PTY LTD, Melbourne

Olmstead RG, Palmer JD (1992) A chloroplast DNA phylogeny of the Solanaceae: subfamily relationships and character evolution. Ann Mo Bot Gard 79:346–360

Prego I, Maldonado S, Otegui M (1998) Seed structure and localization of reserves in *Chenopodium quinoa*. Ann Bot 82:481–488

Sanders PM, Bui AQ, Le BH, Goldberg RB (2005) Differentiation and degeneration of cells that play a major role in tobacco anther dehiscence. Sex Plant Reproduction 17:219–241

Staehelin LA, Newcomb EH (2000) Membrane structure and membranous organelles. In: Buchanan BB, Gruissem W, Jones RL (eds) Biochemistry & molecular biology of plants. American Society of Plant Physiologists, Rockville, Maryland, pp 1–50

Trull MC, Holaway BL, Friedman WE, Malmberg RL (1991) Developmentally regulated antigen associated with calcium crystals in tobacco anthers. Planta 186:13–16

USDA, ARS, National Genetic Resources Program. Germplasm Resources Information Network. (GRIN). National Germplasm Resources Laboratory, Beltsville, Maryland (2008). http://www.ars-grin.gov/cgi-bin/npgs/html/index.pl?language=en. Accessed 11 December 2009

Xie A, Shen Y, Ma D, Huang F, Qiu L, Li S, Chen L (2007) Growth of calcium oxalate crystals induced by complex films containing biomolecules. Cryst Res Technol 42:667–672

Xingxiang L, Zhang D, Linch-Holm VJ, Okita TW, Franceschi VR (2003) Isolation of a crystal matrix protein associated with calcium oxalate precipitation in vacuoles of specialized cells. Plant Physiol 133:549–559